



# Annealing-induced phase conversion on spray pyrolyzed cubic-SnS thin films

T. R. Kishore Bhat<sup>1</sup>, K. Jeganath<sup>1</sup>, Sajan D. George<sup>2</sup>, and Y. Raviprakash<sup>1,\*</sup> 

<sup>1</sup>Semiconductor and Photovoltaics Lab, Department of Physics, Manipal Institute of Technology, Manipal Academy of Higher Education, Manipal 576104, India

<sup>2</sup>Centre for Applied Nanosciences, Department of Atomic and Molecular Physics, Manipal Academy of Higher Education, Manipal, Karnataka 576104, India

Received: 6 January 2023

Accepted: 21 February 2023

Published online:  
13 March 2023

© The Author(s) 2023

## ABSTRACT

The cubic-tin sulfide (SnS) compound material is optimal for the absorber layer in photovoltaic technology. In this study, the role of annealing temperature on the physical properties of cubic-SnS thin film has been determined. The spray pyrolyzed SnS thin films were post-annealed, using the chemical vapor deposition system, at the temperature range between 350 and 500 °C. The annealed films have been analyzed using a comprehensive range of characterization techniques i.e., X-ray diffraction (XRD), Raman spectroscopy, UV–Vis spectroscopy, Photoluminescence spectroscopy (PL), Field-emission scanning electron microscopy (FESEM), Energy dispersive spectroscopy (EDS) and Hall measurements. The XRD results discovered the phase deterioration of cubic-SnS at higher annealing temperatures i.e., > 350 °C. Further, the Raman analysis confirmed the cubic-SnS phase deterioration, along with the formation of SnS<sub>2</sub> and Sn<sub>2</sub>S<sub>3</sub> secondary phases, at higher annealing temperatures. Besides that, a band gap in the range of 1.63–1.68 eV has been obtained for the SnS thin films. The films exhibit the near-band edge emission peak in the PL spectra. Moreover, the SEM micrographs show the needle-shaped grains, and their size and distribution were increased with respect to the enhancement in annealing temperature. A considerable amount of sulfur inclusion was observed in EDS analysis and the films annealed at 450° exhibit the near stoichiometric composition ratio of Sn/S = 1.01. The hall measurement studies showed resistivity, carrier concentration, and mobility of 29.4–376.5 Ω cm, 4.2 × 10<sup>14</sup>–3.0 × 10<sup>16</sup> cm<sup>-3</sup> and 13.1–66.1 cm<sup>2</sup>/Vs, respectively.

Address correspondence to E-mail: raviprakash.y@manipal.edu

## 1 Introduction

Thin film photovoltaic technologies entice researchers interest owing to their direct band gap and higher absorption coefficient in comparison with existing silicon photovoltaic technologies [1–3]. Tin Sulfide (SnS) is a binary semiconductor compound, and it has been used as a light-absorbing layer in Photovoltaics (PV). SnS has been considered a significant material in photovoltaic technology because of the higher absorption coefficient of  $> 10^4 \text{ cm}^{-1}$  and suitable band gap i.e., 1.3–1.8 eV [4, 5]. In addition to that, the elements present in tin sulfide compounds are earth-abundant and environmentally benign compared to well-established, thin-film photovoltaic technologies such as CIGS and CdTe [6, 7]. The aforementioned qualities of SnS material are extremely beneficial for photovoltaic technology. Moreover, the theoretical studies showed that SnS-based photovoltaics have the ability to reach the power conversion efficiency (PCE) of 32% [4]. Thus far, Sinsersuksakul et. al experimentally achieved a PCE of  $\sim 4.3\%$  using the atomic layer deposition technique [8]. The noticed deficiency of SnS photovoltaic devices chiefly occurs because of the defects and band misalignment in the p-n interface [8, 9]. Hence, researchers around the world working enormously to enhance the PCE of SnS photovoltaics.

The crystal structure has a predominant role to decide the properties of the material. The SnS material shows the formation of polymorph crystal structure i.e., orthorhombic ( $\alpha$ -SnS), cubic ( $\pi$ -SnS), and zinc blende [5, 6, 10]. Among that, the orthorhombic SnS is a ground-state crystal structure and the cubic-SnS phase corresponds to a metastable crystal structure [11]. In that, the cubic-SnS ( $\pi$ -SnS) phase has been experimentally discovered in the last decade [12, 13]. The cubic-SnS shows a higher band gap and dielectric constant compared to the orthorhombic-SnS crystal structure and it can facilitate better PCE of the PV device [11, 14, 15]. Therefore, different strategies have been tried by researchers to develop the properties of a cubic-SnS thin film.

Several deposition techniques such as thermal evaporation [16] chemical bath deposition [17], aerosol-assisted chemical vapor deposition [18] and spray pyrolysis deposition [19] was employed to deposit cubic-SnS thin films. Among these, spray pyrolysis possesses a facile and low-cost approach for

the deposition of films. Further, its ability to synthesize films on a large scale facilitates industrial-scale production. Hence in this study, the cubic-SnS thin films were synthesized using the spray pyrolysis technique.

Various strategies have been employed by researchers to ameliorate the properties of cubic-SnS thin films. Among that, post-annealing is considered a constructive approach to enhance the performance of cubic-SnS thin films. The annealing time and temperature role has been investigated for the chemically deposited cubic-SnS thin films by U. Chalapathi et al. [20]. The annealing has been carried out in a nitrogen atmosphere with the occurrence of sulfur. The annealing temperature below 300 °C for 10 min facilitated the cubic-SnS growth with higher crystallinity. Nicolae Spalatu et al. investigated the role of post-deposition temperature and atmosphere for orthorhombic-SnS thin films. The films annealed at 450 °C in the  $\text{SnCl}_2$  atmosphere exhibited an enhanced PCE of 2.8% over the films annealed at other temperatures [21]. Malkeshkumar Patel et al. investigated the annealing temperature on spray pyrolyzed orthorhombic-SnS thin films [22]. The annealing temperature of 500 °C in an argon atmosphere results in enhancement in the film's crystallinity and electrical conductivity. Polivtseva et al. studied the importance of the annealing atmosphere of the spray pyrolyzed cubic-SnS thin films. The phase change in the crystal structure such as  $\text{SnO}_2$ ,  $\text{Sn}_2\text{S}_3$ , and orthorhombic-SnS has been noticed for the annealed films [19]. The above reports elucidate the significance of post-deposition annealing on SnS thin films. Therefore, a post-annealing study is very crucial to ameliorate the performance of absorber layer.

However, to the best of our knowledge, the study of the post-annealing temperature on spray pyrolyzed cubic-SnS thin films has not been determined so far. Therefore, the present work articulates the influence of post-annealing temperature on spray pyrolyzed cubic-SnS thin films. A comprehensive range of characterization techniques has been utilized to investigate the properties of annealed SnS thin film. From the results, the higher annealing temperature leads to the deterioration of cubic-SnS crystal structure and facilitates the formation of  $\text{SnS}_2$  and  $\text{Sn}_2\text{S}_3$  secondary phases. Consequently, the variation in the cubic-SnS thin film's physical properties has been discussed.

## 2 Experimental details

The spray pyrolysis technique was utilized to deposit the SnS thin film. The stannous chloride dihydrate ( $\text{SnCl}_2 \cdot 2\text{H}_2\text{O}$ ) and thiourea ( $\text{CH}_4\text{N}_2\text{S}$ ) were used as initial precursors with the molar concentration of 0.05 M and 0.065 M, respectively. The aqueous solution has been used to prepare the precursors. The soda lime-glass substrate was used, and its temperature is kept at 325 °C. Subsequently, the spray nozzle is used to spray the precursor solution to the substrate and compressed air (pressure-1.2 bar) was employed as a carrier gas during the deposition.

The chemical vapor deposition (CVD) technique was utilized to anneal the as-deposited thin films. The annealing has been performed with the presence of 30 mg elemental sulfur in a quartz boat. Prior to the annealing, the vacuum pressure of  $2 \times 10^{-2}$  mbar has been maintained in the quartz tube then the argon gas has been filled to create an inert atmosphere. The SnS films were annealed at the temperature of 350, 400, 450, and 500 °C for 20 min. The annealed samples were denoted as PA-350, PA-400, PA-450, and PA-500, respectively.

### 2.1 Characterization of thin films

Rigaku mini flex 600 instruments with Cu-K $\alpha$  radiation with  $\lambda = 1.5406 \text{ \AA}$  were utilized to record the X-ray diffraction pattern. Further, the i-Raman plus (B& W Tek Raman spectrometer) has been used to obtain the Raman spectra with the backscattering configuration. The Raman spectra have been recorded using the excitation wavelength of 785 nm. The UV-vis spectrum is recorded at the wavelength range between 190–1100 nm using UV-Shimadzu 1800 spectrometer. The morphology study was carried out using a field-emission scanning electron microscope (Zeiss sigma) and the elemental analysis has been quantified using oxford energy dispersive spectroscopy. The photoluminescence spectra (PL) have been measured at room temperature using Jasco spectrofluorometer FP 8500. Further, the van der Pauw technique has been performed at room temperature to determine resistivity, mobility, and carrier concentration.

## 3 Results and discussion

### 3.1 X-ray diffraction

Figure 1 depicts the XRD pattern of the as-deposited and annealed SnS thin films. The obtained diffractogram has been compared with the standard polymorphs i.e., orthorhombic-SnS (JCPDS Card No. 39-0354) and cubic-SnS structure and possible secondary phases such as  $\text{Sn}_2\text{S}_3$  (JCPDS Card No. 75-2183) and  $\text{SnS}_2$  (JCPDS Card No. 23-06577). The obtained XRD peaks of as-deposited thin film match with a standard cubic-SnS phase. Further, the characteristic peaks at (400), (410), and (300) planes provide a notable difference from the ground state orthorhombic ( $\alpha$ -SnS) and confirm the formation of the cubic-SnS metastable phase [14, 23–25]. Moreover, as-deposited cubic-SnS thin films exhibit phase formation without the occurrence of secondary phases.

Table 1 shows the evaluated parameters from the XRD pattern. The as-deposited SnS films exhibited a crystallite size of 20 nm, and it is found to increase to 22 nm for the films annealed at 350 °C. Further, enhancement in the crystallite size has been noticed to 24 nm at 400 °C annealing temperature. However, the minor presence of the  $\text{SnS}_2$  secondary phase peak

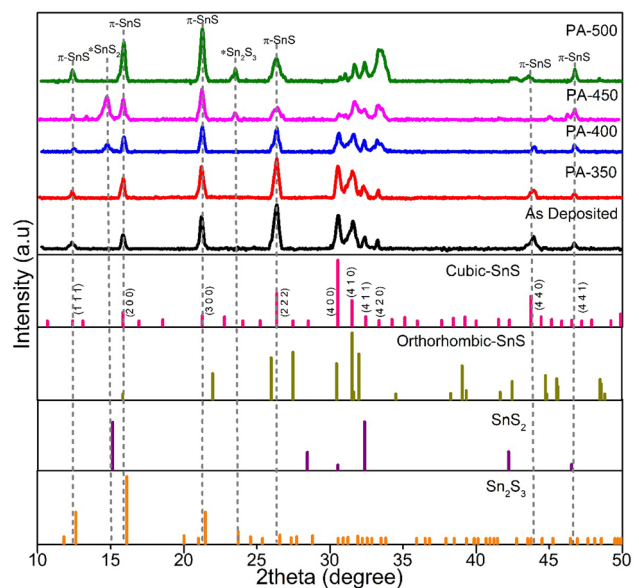


**Fig. 1** XRD pattern of as-deposited and annealed SnS thin films

**Table 1** The crystallite size, dislocation density, and microstrain of the as-deposited and annealed cubic SnS thin films

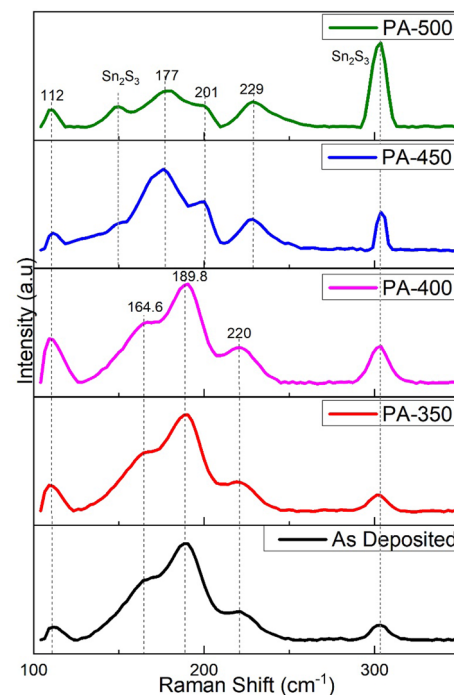
Sample	Peak position (°)	FWHM (°)	Crystallite size (nm)	Dislocation density ( $\text{m}^{-2}$ ) ( $\times 10^{15}$ )	Micro strain ( $\times 10^{-3}$ )
As Deposited	26.0	0.40	20	2.2	1.73
PA-350	26.2	0.37	22	1.9	1.61
PA-400	26.0	0.34	24	1.6	1.48
PA-450	26.5	0.48	17	3.1	2.04
PA-500	26.0	0.50	16	3.5	2.16

occurred in the XRD pattern at a diffraction angle of  $\sim 15^\circ$ . Further improvement in the annealing temperature to 450 °C and 500 °C leads to a reduction of crystallite size to 17 nm and 16 nm, respectively. Besides that, the presence of  $\text{SnS}_2$  and  $\text{Sn}_2\text{S}_3$  secondary phases has been noticed at annealing temperatures of 450 °C and 500 °C, respectively, and their peak intensity has increased significantly. Further, the triple peaks at the plane of (400), (410), and (300) show deterioration, which implies the phase conversion of cubic-SnS crystal structure for films annealed at a higher temperature.

The secondary phases have been noticed in the XRD pattern for the films annealed above 350 °C. The noticed secondary phase and changes in the peak magnitude indicate phase conversion of cubic-SnS. The thermal instability in accordance with the higher volatility of SnS material might be the cause for the noticed deterioration of the cubic-SnS crystal structure. The films annealed above 350 °C led to Sn disproportionation and which causes the deterioration of the cubic-SnS phase and facilitates secondary phase formation i.e.,  $\text{SnS}_2$  and  $\text{Sn}_2\text{S}_3$  [1, 22].

### 3.2 Raman spectroscopy

Figure 2 depicts recorded Raman spectra of the SnS thin films. Raman spectroscopy is a sensitive tool for the determination of secondary phases as compared to XRD. The noticed vibrational modes of  $112 \text{ cm}^{-1}$ ,  $165 \text{ cm}^{-1}$ ,  $177 \text{ cm}^{-1}$ ,  $190 \text{ cm}^{-1}$ ,  $201 \text{ cm}^{-1}$ ,  $220 \text{ cm}^{-1}$ , and  $229 \text{ cm}^{-1}$  nearly match with cubic-SnS and corroborates the phase formation [18, 26]. The phonon confinement might be the cause for the noticed broad peaks in the Raman spectra [13]. All the samples exhibit the Raman vibrational mode at  $306 \text{ cm}^{-1}$ , which is ascribed to the  $\text{Sn}_2\text{S}_3$  secondary phase [27]. The existence of a minor secondary phase has been noticed in the Raman spectra of an as-deposited thin

**Fig. 2** Raman spectrum of as-deposited and annealed SnS thin films

film. In the XRD pattern, the aforementioned secondary phases have not been obtained. The higher detection limit of Raman spectra might effectively probe the occurrence of minor secondary phases over the XRD technique. The intensity of the  $\text{Sn}_2\text{S}_3$  vibrational mode increases corresponding to the increase in the annealing temperature. Concurrently, the cubic-SnS Raman vibrational mode intensity is found to be reduced. A significant change in the Raman shift position has been noticed for the films annealed above 400 °C. The above result indicates phase conversion of the cubic-SnS above the annealing temperature of 400 °C. Overall, the Raman spectra results are in good accordance with the XRD pattern.

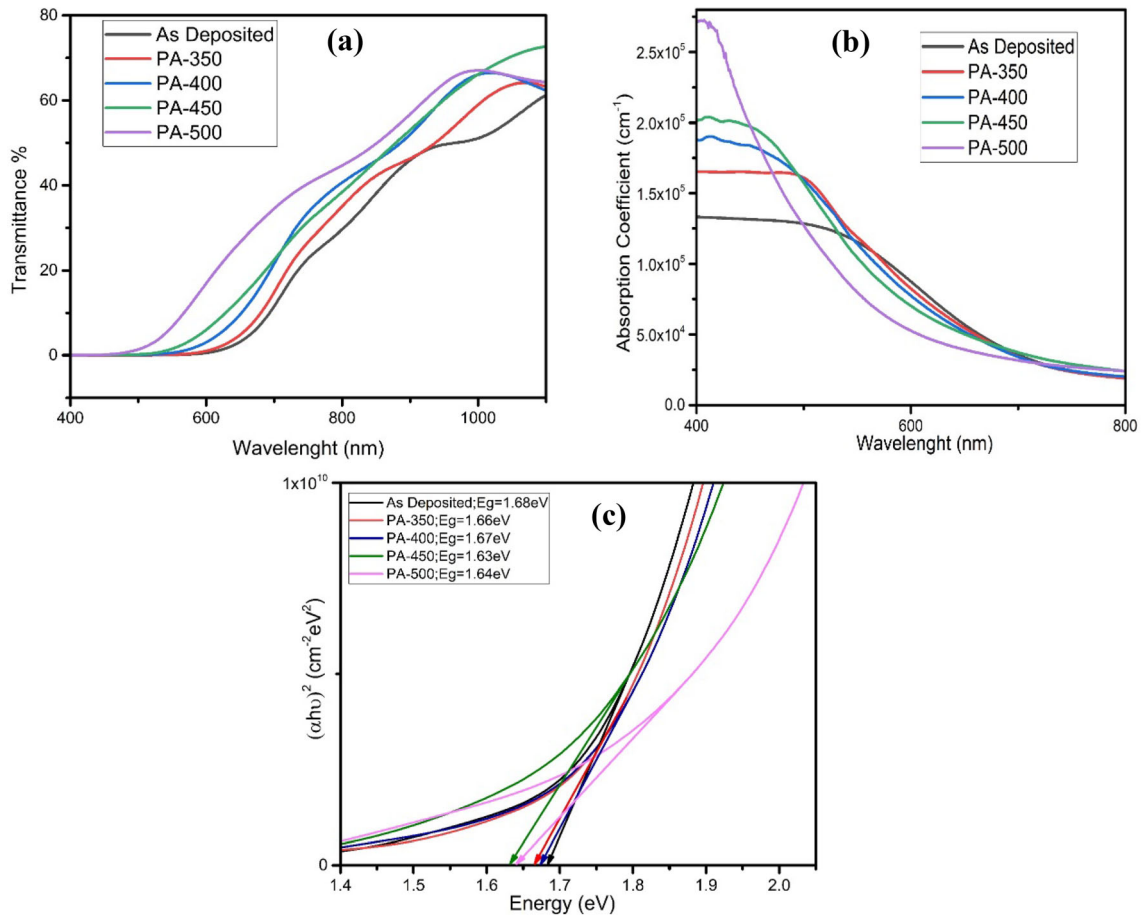


**Fig. 3** a Transmittance, b absorption coefficient, and c Tauc's plot of the cubic SnS thin films

### 3.3 UV-Vis Spectroscopy

Figure 3a and b depict the transmittance and absorption coefficient spectra of SnS thin films. The transmittance percentage in the visible region i.e., 400–700 nm is found to be increased corresponding to a rise in annealing temperature. All the thin films exhibit an absorption coefficient of  $\sim 10^4 \text{ cm}^{-1}$  and it is optimal for the absorber layer. The noticed changes in the transmittance and absorption coefficient might correspond to the change in the crystallinity and the secondary phase formation [28].

The band gap ( $E_g$ ) was determined using the Tauc relation [29]. Figure 3c. depicts the tauc plot of SnS thin films and the direct band gap of 1.63–1.68 eV has been obtained. The as-deposited SnS thin films exhibit a wider band gap of 1.68 eV and it is getting narrow for the annealed films at 350–500 °C. The

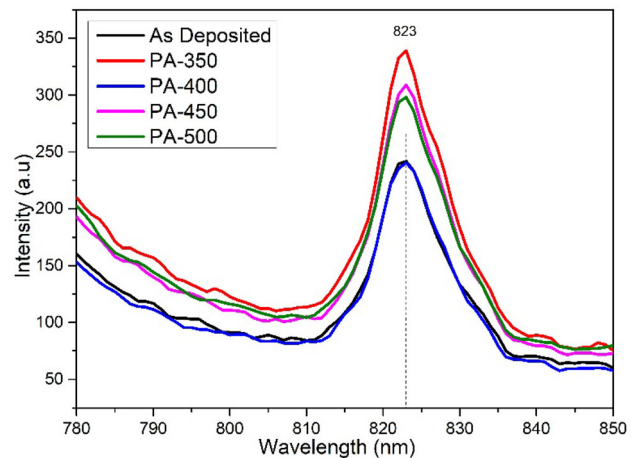


**Fig. 4** Photoluminescence spectra of as-deposited and annealed SnS thin films

obtained band gap value matches with the previous reports [23, 30]. Further, the noticed reduction of band gap for annealed films might be attributed to the reduction of cubic-SnS phase and the secondary phase formation.

### 3.4 Photoluminescence (PL) spectroscopy

The PL spectra of SnS thin films have been depicted in Fig. 4. The occurrence of defect states, within the SnS thin films, has been probed via PL spectra. The excitation wavelength of 723 nm was used to study photoluminescence. All the films exhibit a peak at 823 nm, that corresponds to near-band edge emission [31, 32]. The noticed peak at 823 nm (1.50 eV) is within the range of the evaluated band gap from UV  $\sim$  1.68 eV. Hence, the peak might belong to the defect states present within the band gap. Further,

the sample annealed at 350 °C shows a higher intense peak, which implies a higher level of defect states in comparison with the other annealed films [33].

### 3.5 Field emission scanning electron microscopy (FESEM)

The micrographs of SnS films are presented in Fig. 5. All the films exhibited pinhole and void-free surfaces, which is optimal for the absorber layer performance. Further, the surface region shows the occurrence of needle-shaped grains. The distribution and size of needle-shaped grains have improved at higher annealing temperatures. Moreover, the annealing at 450 °C and 500 °C leads to a higher distribution of needle-shaped grains as compared to the other annealed films.

**Fig. 5** SEM micrographs of as-deposited and annealed cubic SnS thin films

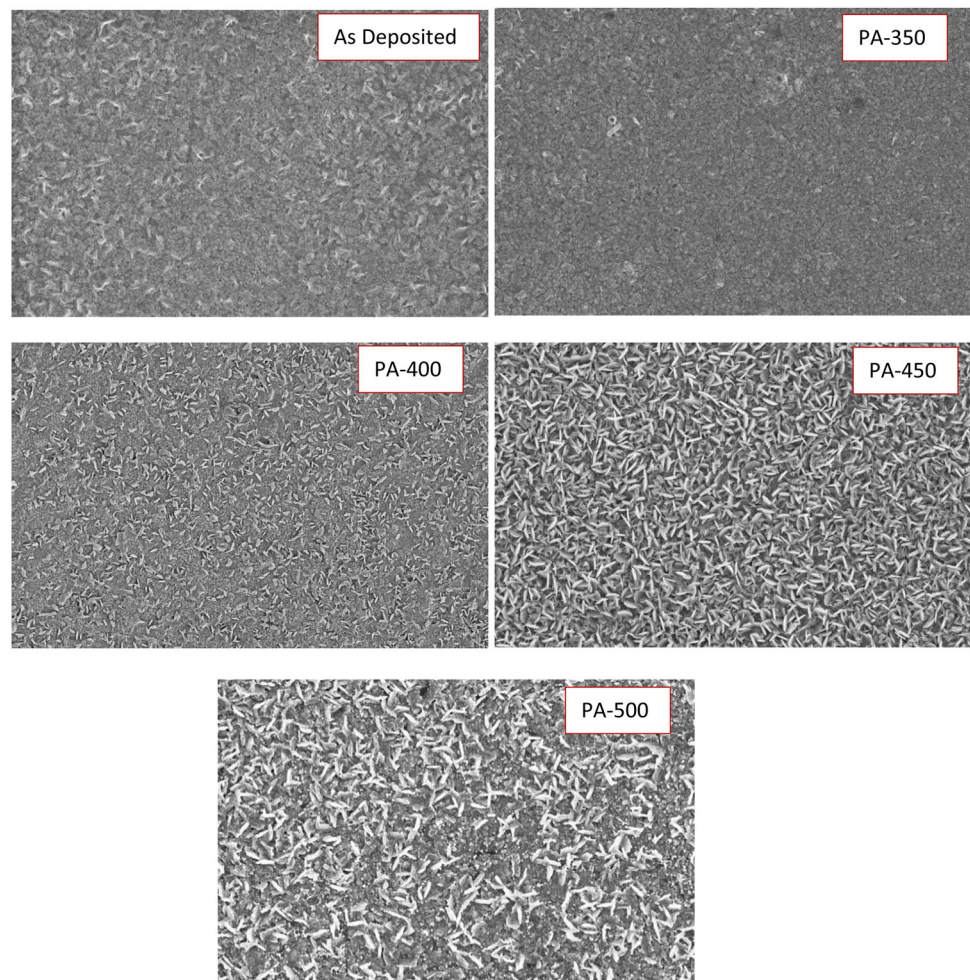


**Table 2** The elemental percentage and the composition ratio of as-deposited and annealed SnS thin films

Sample	Elements (at.%)		Sn/S
	Sn (at.%)	S (at.%)	
As deposited	57.4	42.6	1.34
PA-350	57.0	42.9	1.32
PA-400	55.5	44.5	1.24
PA-450	50.5	49.5	1.01
PA-500	58.7	41.3	1.42

### 3.6 Energy dispersive spectroscopy (EDS)

The elemental percentage and its composition are given in Table. 2. The as-deposited SnS thin films consist of a composition ratio of Sn/S = 1.34. The usual trend of reduction in the elemental percentage of sulfur was noticed for spray pyrolyzed SnS thin films, which corresponds to the evaporation of volatile SO<sub>2</sub> [34]. Further, the increase in the sulfur atomic percentage has been noticed for the annealed films, which is ascribed to the inclusion of sulfur. The near-stoichiometric composition ratio i.e., Sn/S = 1.01 has been obtained for the annealed films at 450 °C. The noticed higher elemental inclusion of sulfur might correspond to the saturated vapor pressure of sulfur. Further, the SnS material exhibits less thermal stability, hence it might cause decomposition during higher temperatures. Thus, the thin films annealed at 500 °C showed an enhancement in the composition ratio of Sn/S = 1.42 [28].

### 3.7 Electrical studies

The van der Pauw technique has been employed to examine the electrical properties of thin films. Table. 3. and Fig. 6. show the obtained resistivity, carrier concentration and mobility of all the SnS thin films. The resistivity of around 3.1 Ω. cm was noticed for the as-deposited SnS thin films. The resistivity is found to be increased to 29.4 Ω. cm and 376.5 Ω. cm

**Table 3** The resistivity, mobility and carrier concentration of as-deposited and annealed SnS thin films

Sample	Resistivity (Ω. cm)	Mobility (cm <sup>2</sup> /V.s)	Carrier Concentration (cm <sup>-3</sup> )
As deposited	3.1	64.3	3.0 × 10 <sup>16</sup>
PA-350	29.4	13.1	1.6 × 10 <sup>16</sup>
PA-400	376.5	38.8	4.2 × 10 <sup>14</sup>
PA-450	34.1	66.1	2.7 × 10 <sup>15</sup>
PA-500	354.9	14.9	1.1 × 10 <sup>15</sup>

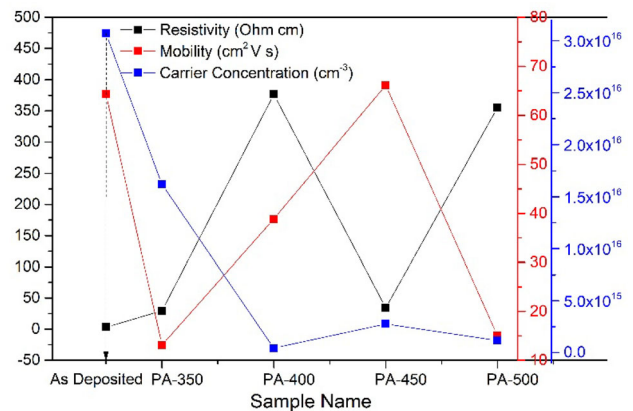


**Fig. 6** The resistivity, mobility and carrier concentration of as-deposited and annealed SnS thin films

for the films annealed at 350 and 400 °C, respectively. A noticed reduction in the Sn/S composition ratio might be the cause for the higher resistivity of the aforementioned SnS thin films. Further, improvement in the annealing temperature to 450 °C leads to a reduction in resistivity i.e., 34.1 Ω cm. The occurrence of SnS<sub>2</sub> secondary phase and the near-stoichiometric ratio of Sn/S might be the cause for the noticed reduction in its resistivity [35]. Further enhancement in the annealing temperature to 500 °C shows an increase in resistivity i.e., 354.9 Ω. cm, which might be attributed to the higher Sn/S ratio = 1.42 and the occurrence of secondary phase i.e., Sn<sub>2</sub>S<sub>3</sub>. The mobility and carrier concentration has found to vary in the range between 13.1 and 66.1 cm<sup>2</sup>/Vs and 4.2 × 10<sup>14</sup>–3.0 × 10<sup>16</sup> cm<sup>-3</sup>, respectively. The obtained variation in mobility and carrier concentration of annealed SnS thin films might be ascribed to the change in composition ratio and crystallinity.

## 4 Conclusion

In summary, the influence of post-annealing temperature on spray pyrolyzed cubic-SnS thin film has been investigated. The cubic-SnS phase has been

found to deteriorate for the films annealed above 350 °C. The occurrence of secondary phases such as Sn<sub>2</sub>S<sub>3</sub> and SnS<sub>2</sub> was increased at a higher temperature. Further, Raman spectroscopy followed the XRD pattern and confirmed a phase deterioration of the cubic-SnS phase at a higher annealing temperature. The thermal instability of SnS, at higher temperatures, led to the noticed phase deterioration. All the thin films exhibit a direct band gap between 1.63 and 1.68 eV. Further, PL spectra showed the near band edge emission, which indicates the higher quality SnS thin films with less deep defects. Further, the SEM micrographs showed the needle shape grain, and their distribution and size were increased at the higher annealing temperature. A significant amount of S inclusion has been noticed for annealed films and at 450 °C a near-stoichiometric composition ratio of Sn/S = 1.01 was obtained. Further, the annealed films exhibit significant changes in resistivity, mobility, and carrier concentration. The above results will provide insight into the cubic-SnS phase conversion and its physical properties corresponding to the post-deposition annealing process and thus enhance the PV device performance.

## Author contributions

The material synthesis, characterization and data analysis were performed by TRKB and KJ. The Raman characterization and the manuscript correction were carried out by SDG. George. The conceptualization, data verification and manuscript correction were done by YR.

## Funding

Open access funding provided by Manipal Academy of Higher Education, Manipal. This work was supported by the Department of Science and Technology (DST) under the Science and Engineering Research Board (SERB), Govt. of India (EMR/2017/002575).

## Data availability

The data pertaining to this report can be provided on a reasonable request.

## Declarations

**Conflict of interest** The authors have no conflict of interest to declare.

**Ethical approval** Not applicable.

**Informed consent** The authors have duly approved the manuscript.

**Open Access** This article is licensed under a Creative Commons Attribution 4.0 International License, which permits use, sharing, adaptation, distribution and reproduction in any medium or format, as long as you give appropriate credit to the original author(s) and the source, provide a link to the Creative Commons licence, and indicate if changes were made. The images or other third party material in this article are included in the article's Creative Commons licence, unless indicated otherwise in a credit line to the material. If material is not included in the article's Creative Commons licence and your intended use is not permitted by statutory regulation or exceeds the permitted use, you will need to obtain permission directly from the copyright holder. To view a copy of this licence, visit <http://creativecommons.org/licenses/by/4.0/>.

## References

1. M. Guc, J. Andrade-Arvizu, I.Y. Ahmet, F. Oliva, M. Placidi, X. Alcobé, E. Saucedo, A. Pérez-Rodríguez, A.L. Johnson, V. Izquierdo-Roca, Structural and vibrational properties of  $\alpha$ - and  $\pi$ -SnS polymorphs for photovoltaic applications. *Acta Mater.* **183**, 1–10 (2020). <https://doi.org/10.1016/j.actamat.2019.11.016>
2. R.N. Mohan, M.T.S. Nair, P.K. Nair, Thin film Sn<sub>2</sub>S<sub>3</sub> via chemical deposition and controlled heating—its prospects as a solar cell absorber. *Appl Surf Sci.* **504**, 144162 (2020). <https://doi.org/10.1016/j.apsusc.2019.144162>
3. K.S. Gour, V. Karade, P. Babar, J. Park, D.M. Lee, V.N. Singh, J.H. Kim, Potential role of kesterites in development of earth-abundant elements-based next generation technology. *Sol. RRL* **2000815**, 1–22 (2021). <https://doi.org/10.1002/solr.202000815>
4. R. Dahule, C.C. Singh, K. Hongo, R. Maezono, E. Panda, Anomalies in the bulk and surface electronic properties of SnS: effects of native defects. *J. Mater. Chem. C* **10**, 5514–5525 (2022). <https://doi.org/10.1039/d1tc04738h>

5. F. Kawamura, Y. Song, H. Murata, H. Tampo, T. Nagai, T. Koida, M. Imura, N. Yamada, Tunability of the bandgap of SnS by variation of the cell volume by alloying with A.E. elements, *Sci Rep.* **12** (2022) 7434. <https://doi.org/10.1038/s41598-022-11074-2>.
6. I. Suzuki, S. Kawanishi, T. Omata, H. Yanagi, Current status of n-type SnS: paving the way for SnS homojunction solar cells. *J. Phys.* **4**, 042002 (2022). <https://doi.org/10.1088/2515-7655/ac86a1>
7. D.G. Moon, S. Rehan, D.H. Yeon, S.M. Lee, S.J. Park, S.J. Ahn, Y.S. Cho, A review on binary metal sulfide hetero-junction solar cells. *Sol. Energy Mater. Solar Cells* **200**, 9963 (2019). <https://doi.org/10.1016/j.solmat.2019.109963>
8. P. Sinsersuksakul, L. Sun, S.W. Lee, H.H. Park, S.B. Kim, C. Yang, R.G. Gordon, Overcoming efficiency limitations of SnS-based solar cells. *Adv. Energy Mater.* **4**, 1–7 (2014). <https://doi.org/10.1002/aenm.201400496>
9. R.E. Banai, M.W. Horn, J.R.S. Brownson, A review of tin (II) monosulfide and its potential as a photovoltaic absorber. *Sol. Energy Mater. Sol. Cells* **150**, 112–129 (2016). <https://doi.org/10.1016/j.solmat.2015.12.001>
10. Y. Zi, J. Zhu, L. Hu, M. Wang, W. Huang, Nanoengineering of Tin monosulfide (SnS)-based structures for emerging applications. *Small Sci.* **2**, 2100098 (2022). <https://doi.org/10.1002/smssc.202100098>
11. J.M. Skelton, L.A. Burton, F. Oba, A. Walsh, Metastable cubic tin sulfide: a novel phonon-stable chiral semiconductor. *APL Mater.* **5**, 036101 (2017). <https://doi.org/10.1063/1.4977868>
12. A. Rabkin, S. Samuha, R.E. Abutbul, V. Ezersky, L. Meshi, Y. Golan, New nanocrystalline materials: a previously unknown simple cubic phase in the SnS binary system. *Nano Lett.* **15**, 2174–2179 (2015). <https://doi.org/10.1021/acs.nanolett.5b00209>
13. R.E. Abutbul, E. Segev, L. Zeiri, V. Ezersky, G. Makovab, Y. Golan, Synthesis and properties of nanocrystalline  $\pi$ -SnS-a new cubic phase of tin sulphide. *RSC Adv.* **6**, 5848–5855 (2016). <https://doi.org/10.1039/C5RA23092F>
14. V.E.G. Flores, M.T.S. Nair, P.K. Nair, Thermal stability of ‘metastable’ cubic tin sulfide and its relevance to applications. *Semicond. Sci. Technol.* **33**, 1–27 (2016)
15. S.U. Rehman, F.K. Butt, B. UlHaq, S. AlFaify, W.S. Khan, C. Li, Exploring novel phase of tin sulfide for photon/energy harvesting materials. *Solar Energy.* **169**, 648–657 (2018). <https://doi.org/10.1016/j.solener.2018.05.006>
16. K.O. Hara, S. Suzuki, N. Usami, Formation of metastable cubic phase in SnS thin films fabricated by thermal evaporation. *Thin Solid Films* **639**, 7–11 (2017). <https://doi.org/10.1016/j.tsf.2017.08.025>
17. U. Chalapathi, B. Poornaprakash, S.H. Park, Chemically deposited cubic SnS thin films for solar cell applications. *Sol. Energy* **139**, 238–248 (2016). <https://doi.org/10.1016/j.solener.2016.09.046>
18. I.Y. Ahmet, M. Guc, Y. Sánchez, M. Neuschitzer, V. Izquierdo-Roca, E. Saucedo, A.L. Johnson, Evaluation of AA-CVD deposited phase pure polymorphs of SnS for thin films solar cells. *RSC Adv.* **9**, 14899–14909 (2019). <https://doi.org/10.1039/c9ra01938c>
19. S. Polivtseva, A. Katerski, E. Kärber, I. Oja Acik, A. Mere, V. Mikli, M. Krunks, Post-deposition thermal treatment of sprayed SnS films. *Thin Solid Films.* **633**, 179–184 (2017). <https://doi.org/10.1016/j.tsf.2017.01.014>
20. U. Chalapathi, B. Poornaprakash, S.H. Park, Effect of post-deposition annealing on the growth and properties of cubic SnS films. *Superlattices Microstruct.* **103**, 221–229 (2017). <https://doi.org/10.1016/j.spmi.2017.01.034>
21. N. Spalatu, J. Hiie, R. Kaupmees, O. Volobujeva, J. Krustok, I.O. Acik, M. Krunks, Postdeposition processing of SnS thin films and solar cells: prospective strategy to obtain large, sintered, and doped SnS grains by recrystallization in the presence of a metal halide flux. *ACS Appl Mater Interfaces* **11**, 17539–17554 (2019). <https://doi.org/10.1021/acsami.9b03213>
22. M. Patel, I. Mukhopadhyay, A. Ray, Annealing influence over structural and optical properties of sprayed SnS thin films. *Opt Mater.* **35**, 1693–1699 (2013). <https://doi.org/10.1016/j.optmat.2013.04.034>
23. E. Barrios-Salgado, L.A. Rodríguez-Guadarrama, A.R. Garcia-Angelmo, J. Campos Álvarez, M.T.S. Nair, P.K. Nair, Large cubic tin sulfide–tin selenide thin film stacks for energy conversion, *Thin Solid Films.* **615** (2016) 415–422. Doi: <https://doi.org/10.1016/j.tsf.2016.07.048>.
24. P.K. Nair, E. Barrios-Salgado, M.T.S. Nair, Cubic-structured tin selenide thin film as a novel solar cell absorber. *Phys. Status Solidi A* **213**, 2229–2236 (2016). <https://doi.org/10.1002/pssa.201533040>
25. M.S. Mahdi, K. Ibrahim, N.M. Ahmed, A. Hmood, S.A. Azzez, F.I. Mustafa, M. Bououdina, Influence of pH value on structural, optical and photoresponse properties of SnS films grown via chemical bath deposition. *Mater. Lett.* **210**, 279–282 (2018). <https://doi.org/10.1016/j.matlet.2017.09.049>
26. O.V. Bilousov, Y. Ren, T. Törndahl, O. Donzel-Gargand, T. Ericson, C. Platzer-Björkman, M. Edoff, C. Häggglund, Atomic layer deposition of cubic and orthorhombic phase tin monosulfide. *Chem. Mater.* **29**, 2969–2978 (2017). <https://doi.org/10.1021/acs.chemmater.6b05323>
27. M.S. Mahdi, A. Hmood, K. Ibrahim, N.M. Ahmed, M. Bououdina, Dependence of pH on phase stability, optical and photoelectrical properties of SnS thin films. *Superlattices*

- Microstruct. **128**, 170–176 (2019). <https://doi.org/10.1016/j.spmi.2019.01.031>
28. K. Jeganath, N.J. Choudhari, G. Shruthi Pai, A. Rao, Y. Raviprakash, Role of substrate temperature on spray pyrolysed metastable  $\pi$ -SnS thin films. *Mater. Sci. Semicond. Process.* **113**, 5050 (2020). <https://doi.org/10.1016/j.mssp.2020.105050>
29. A. Javed, Qurat-ul-Ain, M. Bashir, Controlled growth, structure and optical properties of Fe-doped cubic  $\pi$ -SnS thin films, *J Alloys Compd.* **759**, 14–21 (2018). <https://doi.org/10.1016/j.jallcom.2018.05.158>.
30. U. Chalapathi, B. Poornaprakash, S.H. Park, Growth and properties of cubic SnS films prepared by chemical bath deposition using EDTA as the complexing agent. *J. Alloys Compd.* **689**, 938–944 (2016). <https://doi.org/10.1016/j.jallcom.2016.08.066>
31. B. Ghosh, M. Das, P. Banerjee, S. Das, Fabrication and optical properties of SnS thin films by SILAR method. *Appl. Surf. Sci.* **254**, 6436–6440 (2008). <https://doi.org/10.1016/j.apsusc.2008.04.008>
32. M. Cao, C. Wu, K. Yao, J. Jing, J. Huang, M. Cao, J. Zhang, J. Lai, O. Ali, L. Wang, Y. Shen, Chemical bath deposition of single crystal SnS nanobelts on glass substrates. *Mater. Res. Bull.* **104**, 244–249 (2018). <https://doi.org/10.1016/j.materresbull.2018.03.039>
33. K. Santhosh Kumar, C. Manoharan, S. Dhanapandian, A. Gowri Manohari, Effect of Sb dopant on the structural, optical and electrical properties of SnS thin films by spray pyrolysis technique. *Spectrochim Acta A* **115**, 840–844 (2013). <https://doi.org/10.1016/j.saa.2013.06.112>
34. M.E. Rodriguez, D. Sylla, Y. Sanchez, S. López-Marino, X. Fontané, J. López-García, M. Placidi, A. Pérez-Rodríguez, O. Vigil-Galán, E. Saucedo, Pneumatically sprayed CuZnSnS<sub>4</sub> films under Ar and Ar-H<sub>2</sub> atmosphere. *J Phys D* **47**, 245101 (2014). <https://doi.org/10.1088/0022-3727/47/24/245101>
35. M. Gurubhaskar, N. Thota, M. Raghavender, G. Hema Chandra, P. Prathap, Y.P. Venkata Subbaiah, Influence of sulfurization time on two step grown SnS thin films. *Vacuum* **155**, 318–324 (2018). <https://doi.org/10.1016/j.vacuum.2018.06.011>

**Publisher's Note** Springer Nature remains neutral with regard to jurisdictional claims in published maps and institutional affiliations.